

# Transverse dynamics of Pb–Pb collisions at 40 A GeV/ $c$ viewed by strange hadrons

F Antinori<sup>1</sup>, P Bacon<sup>2</sup>, A Badalà<sup>3</sup>, R Barbera<sup>3</sup>, A Belogianni<sup>4</sup>,  
I J Bloodworth<sup>2</sup>, M Bombara<sup>5</sup>, G E Bruno<sup>6</sup>, S A Bull<sup>2</sup>,  
R Caliendo<sup>6</sup>, M Campbell<sup>7</sup>, W Carena<sup>7</sup>, N Carrer<sup>7</sup>,  
R F Clarke<sup>2</sup>, A Dainese<sup>1‡</sup>, D Di Bari<sup>6</sup>, S Di Liberto<sup>8</sup>, R Divià<sup>7</sup>,  
D Elia<sup>6</sup>, D Evans<sup>2</sup>, G A Feofilov<sup>9</sup>, R A Fini<sup>6</sup>, P Ganoti<sup>4</sup>,  
B Ghidini<sup>6</sup>, G Grella<sup>10</sup>, H Helstrup<sup>11</sup>, K F Hetland<sup>11</sup>,  
A K Holme<sup>12</sup>, A Jacholkowski<sup>3</sup>, G T Jones<sup>2</sup>, P Jovanovic<sup>2</sup>,  
A Jusko<sup>2</sup>, R Kamermans<sup>13</sup>, J B Kinson<sup>2</sup>, K Knudson<sup>7</sup>,  
V Kondratiev<sup>9</sup>, I Králik<sup>5</sup>, A Kravčáková<sup>14</sup>, P Kuijer<sup>13</sup>,  
V Lenti<sup>6</sup>, R Lietava<sup>2</sup>, G Løvhøiden<sup>12</sup>, V Manzari<sup>6</sup>,  
M A Mazzone<sup>8</sup>, F Meddi<sup>8</sup>, A Michalon<sup>15</sup>, M Morando<sup>1</sup>,  
P I Norman<sup>2</sup>, A Palmeri<sup>3</sup>, G S Pappalardo<sup>3</sup>, B Pastirčák<sup>5</sup>,  
R J Platt<sup>2</sup>, E Quercigh<sup>1</sup>, F Riggi<sup>3</sup>, D Röhrich<sup>16</sup>, G Romano<sup>10</sup>,  
R Romita<sup>6</sup>, K Šafařík<sup>7</sup>, L Šándor<sup>5</sup>, E Schillings<sup>13</sup>, G Segato<sup>1</sup>,  
M Sené<sup>17</sup>, R Sené<sup>17</sup>, W Snoeys<sup>7</sup>, F Soramel<sup>1‡</sup>,  
M Spyropoulou-Stassinaki<sup>4</sup>, P Staroba<sup>18</sup>, R Turrisi<sup>1</sup>,  
T S Tveter<sup>12</sup>, J Urbán<sup>14</sup>, P van de Ven<sup>13</sup>, P Vande Vyvre<sup>7</sup>,  
A Vascotto<sup>7</sup>, T Vik<sup>12</sup>, O Villalobos Baillie<sup>2</sup>, L Vinogradov<sup>9</sup>,  
T Virgili<sup>10</sup>, M F Votruba<sup>2</sup>, J Vrláková<sup>14</sup> and P Závada<sup>18</sup>

<sup>1</sup> University of Padua and INFN, Padua, Italy

<sup>2</sup> University of Birmingham, Birmingham, UK

<sup>3</sup> University of Catania and INFN, Catania, Italy

<sup>4</sup> Physics Department, University of Athens, Athens, Greece

<sup>5</sup> Institute of Experimental Physics, Slovak Academy of Science, Košice, Slovakia

<sup>6</sup> Dipartimento IA di Fisica dell'Università e del Politecnico di Bari and INFN, Bari, Italy

<sup>7</sup> CERN, European Laboratory for Particle Physics, Geneva, Switzerland

<sup>8</sup> University “La Sapienza” and INFN, Rome, Italy

<sup>9</sup> State University of St. Petersburg, St. Petersburg, Russia

<sup>10</sup> Dipartimento di Scienze Fisiche “E.R. Caianiello” dell'Università and INFN, Salerno, Italy

<sup>11</sup> Høgskolen i Bergen, Bergen, Norway

<sup>12</sup> Fysisk Institutt, Universitetet i Oslo, Oslo, Norway

<sup>13</sup> Utrecht University and NIKHEF, Utrecht, The Netherlands

<sup>14</sup> P.J. Šafařík University, Košice, Slovakia

<sup>15</sup> IReS/ULP, Strasbourg, France

‡ Present address: Laboratori Nazionali di Legnaro, Legnaro, Italy

† Permanent address: University of Udine, Udine, Italy

<sup>16</sup> Fysisk Institutt, Universitetet i Bergen, Bergen, Norway

<sup>17</sup> Collège de France, Paris, France

<sup>18</sup> Institute of Physics, Prague, Czech Republic

E-mail: Giuseppe.Bruno@ba.infn.it

**Abstract.** The transverse mass spectra of  $K_S^0$ ,  $\Lambda$ ,  $\Xi$  and  $\Omega$  particles produced in Pb–Pb collisions at 40 A GeV/c have been studied for a sample of events corresponding to the most central 53% of the inelastic Pb–Pb cross-section. We analyze the distributions in the framework of a parameterized model inspired by hydrodynamics. The dependence of the freeze-out parameters on particle species and event centrality is discussed and comparisons with results at higher energy are shown.

PACS numbers: 12.38.Mh, 25.75.Nq, 25.75.Ld, 25.75.Dw

## 1. Introduction

Ultra-relativistic collisions between heavy ions are used to study the properties of nuclear matter at high energy density. In particular, lattice Quantum Chromo-Dynamics (QCD) calculations predict a state of matter of deconfined quarks and gluons (quark-gluon plasma, QGP) at an energy density exceeding  $\sim 0.6$  GeV/fm<sup>3</sup> [1]. For recent reviews of experimental results and theoretical developments see references [2].

Strange particle production has proved to be a powerful tool to study the system formed in heavy ion collisions [3]. If a QGP state is formed, an increased production of  $s$  and  $\bar{s}$  quarks with respect to normal hadronic interactions is expected [4]. The abundance of  $s$  and  $\bar{s}$  quarks would equilibrate in a few fm/c, comparable with the plasma lifetime. The result, after statistical hadronization, would be an enhancement of the strange and multi-strange particle abundance in nucleus–nucleus interactions with respect to nucleon–nucleon interactions; the enhancement was also predicted to increase with the number of valence strange quarks [4]. We have reported recently [5] results confirming the WA97 finding [6] that strange particle production in Pb–Pb collisions at 158 A GeV/c is enhanced, with the predicted hierarchy as expected in a QGP scenario. The effect amounts to about a factor 20 enhancement for the triply-strange  $\Omega$ . Preliminary results at 40 A GeV/c [7] indicate a similar pattern of the strangeness enhancement to that observed at higher energy. Enhancement of strange meson and baryon production in Pb–Pb collisions has also been reported by the NA49 Collaboration [8, 9, 10].

Ratios of particle abundances are rather well described by thermal models [11]; this is interpreted as strong evidence of local thermalization of the nuclear matter formed in the collision on a time scale shorter than the lifetime of the fireball. Local thermal equilibrium is a prerequisite to allow the description of the evolution of the system using ideal fluid dynamics, provided that the mean free path of the fireball constituents is short enough. Hydro-dynamics or parameterized models inspired by hydro-dynamics have shown to give a successful description of a number of observables, i.e. transverse

momentum ( $p_T$ ) and rapidity ( $y$ ) distributions, direct and elliptic flow, and two-particle correlation functions (for recent reviews see, e.g., references [12]).

Collective dynamics in the transverse direction is of major interest since it can only arise by the buildup of a pressure gradient which, in turn, would be strongly suggestive of thermal equilibration of the system formed in the collision.

The shapes of the  $p_T$  spectra are expected to be determined by an interplay between two effects: the thermal motion of the particles in the fireball and a pressure-driven radial flow, induced by the fireball expansion. To disentangle the two contributions we rely on the blast-wave model [13], which assumes cylindrical symmetry for an expanding fireball in local thermal equilibrium, under different hypotheses on the transverse flow profile. The analysis of transverse expansion in Pb–Pb at 158 A GeV/c was presented in reference [14]. In this paper we discuss the study of the transverse mass ( $m_T = \sqrt{p_T^2 + m^2}$ ) spectra for  $\Lambda$ ,  $\Xi^-$ ,  $\Omega^-$  hyperons, their anti-particles and  $K_S^0$  measured in Pb–Pb collisions at 40 A GeV/c.

## 2. The NA57 set-up

The  $\Lambda$ ,  $\Xi^-$ ,  $\Omega^-$  hyperons, their anti-particles and the  $K_S^0$  mesons are identified by reconstructing their weak decays into final states containing only charged particles:

$$\begin{aligned}
 K_S^0 &\rightarrow \pi^+ + \pi^- & \Lambda &\rightarrow p + \pi^- \\
 \Xi^- &\rightarrow \Lambda + \pi^- & \Omega^- &\rightarrow \Lambda + K^- \\
 &\quad \downarrow & &\quad \downarrow \\
 &\quad p + \pi^- & &\quad p + \pi^-
 \end{aligned}
 \tag{1}$$

and the corresponding charge conjugates for anti-hyperons. The charged tracks emerging from strange particle decays were reconstructed in a telescope made of an array of silicon detector planes of 5x5 cm<sup>2</sup> cross-section placed in an approximately uniform magnetic field of 1.4 Tesla perpendicular to the beam line; the bulk of the detectors was closely packed in an approximately 30 cm long compact part used for pattern recognition. Descriptions of the NA57 apparatus can be found in references [5, 14, 15]. There, however, emphasis is placed on the 158 A GeV/c beam momentum set-up. The experimental set-up for Pb-Pb collisions at 40 A GeV/c is conceptually similar: the only differences are in the telescope inclination and detector positions which have been chosen in order to optimize at the lower energy the acceptance and reconstruction efficiency of strange particles produced at mid-rapidity. A sketch of the silicon telescope as installed on the NA57 optical bench is shown in figure 1. An inclination angle of 72 mrad with respect to the beam line and a distance of the first pixel plane from the target equal to 40 cm were set in order to accept particles produced in about half a unit of rapidity around central rapidity at medium transverse momentum.

An array of scintillation counters (Petals), placed 7.9 cm downstream of the target, provided a fast signal to trigger on the centrality of the collisions. The Petals covered the pseudo-rapidity region  $0.8 < \eta < 1.8$  and their thresholds could be set so as to accept events with track multiplicities above an adjustable limit. This was tuned so that the

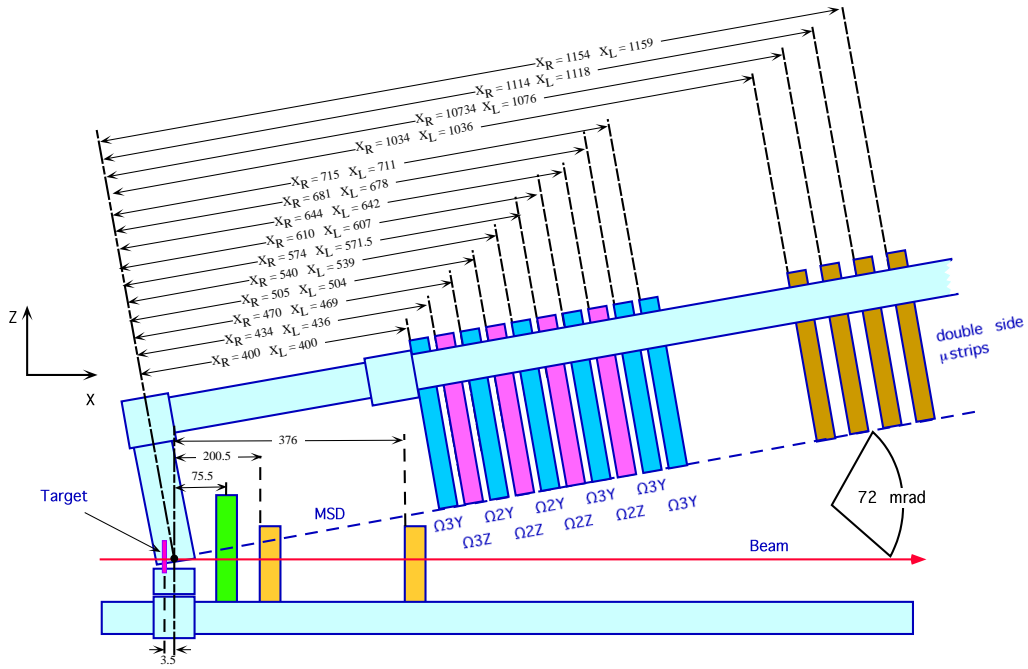


**Figure 1.** Sketch (not to scale) of the NA57 apparatus placed inside the 1.4 T field of the GOLIATH magnet in the 40 A GeV/c set-up. All distances are given in mm.

triggered event sample corresponds to approximately the most central 56% of the Pb–Pb inelastic cross-section. The thickness of the Pb target was 1% of an interaction length.

The centrality of the Pb–Pb collisions is determined (off-line) by analyzing the charged particle multiplicity measured by two stations of micro-strip silicon detectors (MSD) which sample the pseudo-rapidity intervals  $1.9 < \eta < 3$  and  $2.4 < \eta < 3.6$ .

### 3. Data sample and analysis

The results presented in this paper are based on the analysis of the full data sample collected in Pb–Pb collisions at 40 A GeV/c, consisting of 240 M events. The selected sample used for the analysis corresponds to the most central 53% of the inelastic Pb–Pb cross-section. The data sample has been divided into five centrality classes (0,1,2,3 and 4, class 4 being the most central) according to the value of the charged particle multiplicity measured by the MSD. The procedure for the measurement of the multiplicity distribution and the determination of the collision centrality for each class is described in reference [16]. The fractions of the inelastic cross-section for the five classes, calculated assuming an inelastic Pb–Pb cross-section of 7.26 barn, are the same as those defined at higher beam momentum (158 A GeV/c) and they are given in table 1.

The strange particle signals are extracted with the same procedure used at 158 A GeV/c [5, 14] by applying similar geometric and kinematic constraints. The invariant mass spectra of  $\pi^-\pi^+$ ,  $p\pi$ ,  $\Lambda\pi$  and  $\Lambda K$  combinations after all analysis cuts are shown in

**Table 1.** Centrality ranges for the five classes.

Class	0	1	2	3	4
$\sigma/\sigma_{inel}$ (%)	40 to 53	23 to 40	11 to 23	4.5 to 11	0 to 4.5

figure 2. The quality of the signals is comparable to that at 158 GeV/c [5, 14], with the

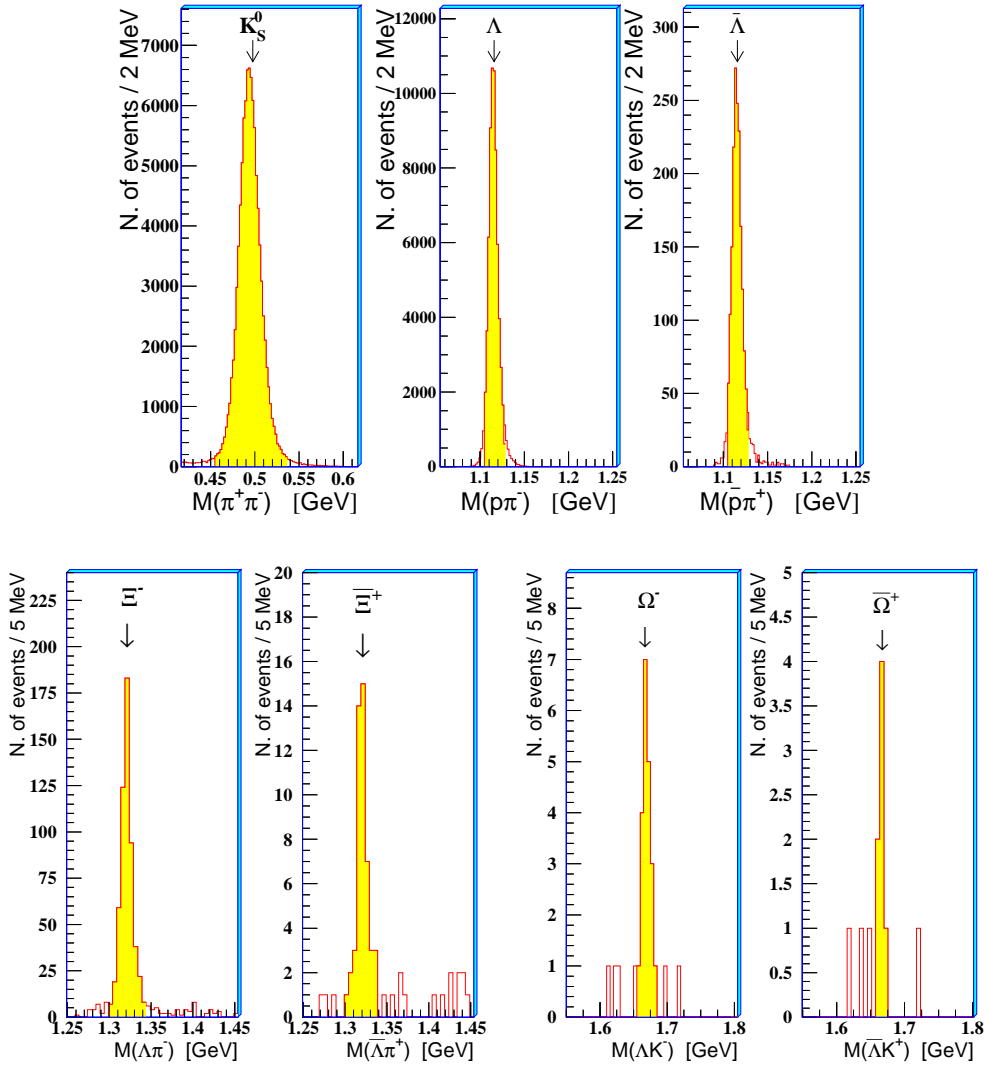


**Figure 2.** Sample invariant mass spectra for  $\pi^+\pi^-$ ,  $p\pi$ ,  $\Lambda\pi$  and  $\Lambda K$ . The arrows show the PDG mass values [17].

hyperon mass peaks at the nominal PDG values [17] and FWHMs of about 15 MeV/ $c^2$ . The  $K_s^0$  invariant mass peak has a FWHM of 25 MeV/ $c^2$  and its maximum is shifted down by 4 MeV/ $c^2$  with respect to the nominal value. This effect has been accounted for in the calculation of the corrections for acceptance and reconstruction inefficiencies. The selected particles have been chosen in the invariant mass intervals corresponding to

the shaded areas of figure 2.

The amount of residual combinatorial background has been evaluated using the event-mixing technique [14, 18]. As an example, figure 3 shows the  $\pi^+\pi^-$  invariant mass distribution for real and mixed events before (left) and after (right) the application of the analysis cuts. For the cascade hyperons, the residual background has been evaluated

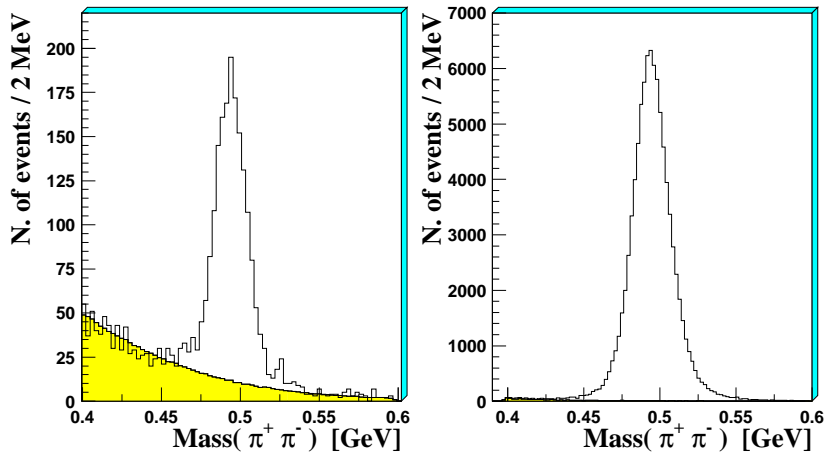


**Figure 3.** The  $\pi^+\pi^-$  invariant mass distribution for a small sample of events before analysis cuts (left) and for the total sample after analysis cuts (right). The shaded histograms show the combinatorial background evaluated by event mixing.

to be about 4% for  $\Xi^-$  and less than 10% for  $\Xi^+$  and  $\Omega^- + \bar{\Omega}^+$ ; for the singly-strange particles, it has been estimated to be 1%, 0.8% and 2% for  $K_S^0$ ,  $\Lambda$  and  $\bar{\Lambda}$ , respectively.

The acceptance regions in the transverse momentum ( $p_T$ ) versus rapidity ( $y$ ) plane are shown in figure 4. The limits of these windows have been defined in order to exclude from the final sample the strange particles whose lines of flight are very close to the borders of the telescope, where the systematic errors are more difficult to evaluate.

Each reconstructed particle is assigned a weight to correct for acceptance and reconstruction inefficiencies. The computational algorithm of the event weight is the same used at higher energy [5, 14]: a number of Monte Carlo events are generated — each event consisting of one simulated particle, with the  $p_T$  and  $y$  of the real particle and random azimuthal and internal decay angles, merged with a real event of similar telescope hit multiplicity as the original event — and they are reconstructed with the same analysis tools as for real events; the final weight is the ratio of the number of generated particles to the number of those reconstructed and retained by the selection criteria. This individual correction procedure has been applied to all the reconstructed  $\Omega$ ,  $\Xi$  and  $\bar{\Lambda}$  particles. For the much more abundant  $K_S^0$  and  $\Lambda$  candidates, the individual weights have been computed for a subsample only. These amount to 1/20 and 1/15 of the total sample, respectively, and they have been extracted uniformly over the full data taking period. The statistics of particles collected and individually corrected is given in table 2.

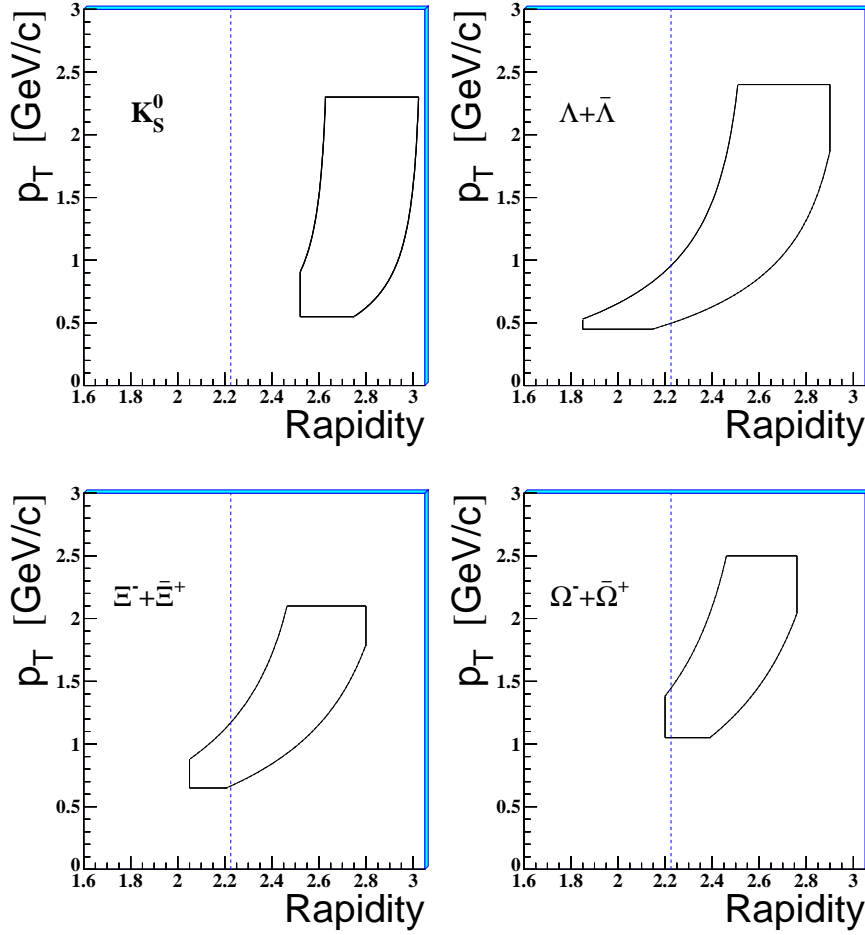


**Figure 4.** The  $p_T$ - $y$  acceptance windows. Dashed lines show the position of mid-rapidity ( $y_{cm} = 2.225$ ).

**Table 2.** Statistics of the collected and weighted particles.

	$K_S^0$	$\Lambda$	$\bar{\Lambda}$	$\Xi^-$	$\bar{\Xi}^+$	$\Omega^- + \bar{\Omega}^+$
total	97000	82500	2100	439	39	28
$\frac{\text{weighted}}{\text{total}}$	1/20	1/15	1	1	1	1

The correction procedure has been extensively checked by comparing real and Monte Carlo distributions for several parameters — in particular those used for particle selection, such as the distance of closest approach in space between the two decay particles, the position of the decay vertices, the impact parameters of the particles $\ddagger$ , etc. — for different data taking periods and magnetic field orientations (up and down).

In order to further check the stability of the results (i.e. the  $\frac{1}{m_\tau} \frac{d^2N}{dm_\tau dy}$  distributions)

$\ddagger$  The impact parameter is approximated as the distance from the primary vertex of the intersection of the measured particle trajectory with a plane transverse to the beam line passing through the target position.

the selection criteria have also been varied, either by changing their limiting values or by excluding them one at a time. As a result of these studies we can estimate the contribution of the selection and correction procedure to the systematic errors on the slope of the  $\frac{1}{m_T} \frac{dN}{dm_T}$  distributions to be about 12% for  $\Omega$  and 8% for all other particles.

The experimental procedure for the determination of the  $m_T$  distribution is described in detail in reference [14], where the results at 158 A GeV/c are discussed. The measured distribution of the double differential invariant cross-section  $\frac{1}{m_T} \frac{d^2N}{dm_T dy}$  has been assumed to factorize into a  $y$  and an  $m_T$  dependent part:

$$\frac{1}{m_T} \frac{d^2N}{dm_T dy}(y, m_T) = f(y) \cdot \frac{1}{m_T} \frac{dN}{dm_T}(m_T). \quad (2)$$

This assumption has been verified by considering the  $m_T$  ( $y$ ) distributions for different slices in rapidity (transverse mass).

The shape of the rapidity distribution, i.e.  $f(y)$  in equation 2, has been found to be well described within our limited acceptance by a constant for all particles except for  $K_S^0$  and  $\bar{\Lambda}$ , where a Gaussian provides a better description. We have reported a similar finding in Pb–Pb collisions at 158 A GeV/c beam momentum [19].

The hypotheses on the factorization of the double differential invariant cross-section (equation 2) and on the shape of the rapidity distributions ( $f(y)$ ) can introduce a systematic bias on the slope of the  $\frac{1}{m_T} \frac{dN}{dm_T}(m_T)$  distributions which has been estimated not to exceed 5%.

An additional source of systematic errors comes from the residual combinatorial background, which can have a different  $m_T$  distribution than the signal. This error is found to be negligible for  $\Lambda$  and  $K_S^0$ , and about 1.5%, 2%, 4% and 7% for  $\bar{\Lambda}$ ,  $\Xi^-$ ,  $\Xi^+$  and  $\Omega$ , respectively.

#### 4. Exponential fits of the transverse mass spectra

The inverse slope parameter  $T_{\text{app}}$  (“apparent temperature”) has been extracted by means of a maximum likelihood fit of the measured double differential invariant cross-section  $\frac{1}{m_T} \frac{d^2N}{dm_T dy}$  to the formula

$$\frac{1}{m_T} \frac{d^2N}{dm_T dy} = f(y) \exp\left(-\frac{m_T}{T_{\text{app}}}\right) \quad (3)$$

The apparent temperature is interpreted as due to the thermal motion coupled with a collective transverse flow of the fireball components [13]. The differential invariant cross-section distributions are shown in figure 5 as a function of  $m_T$  for the most central 53% of the inelastic Pb–Pb cross-section with the likelihood fit results superimposed. The values of the inverse slope parameters  $T_{\text{app}}$  are given in table 3. The quoted systematic errors are obtained by propagating the partial contributions due to i) the selection and correction procedure, ii) the hypothesis on the parameterization of the double differential cross-section and iii) the residual combinatorial background.



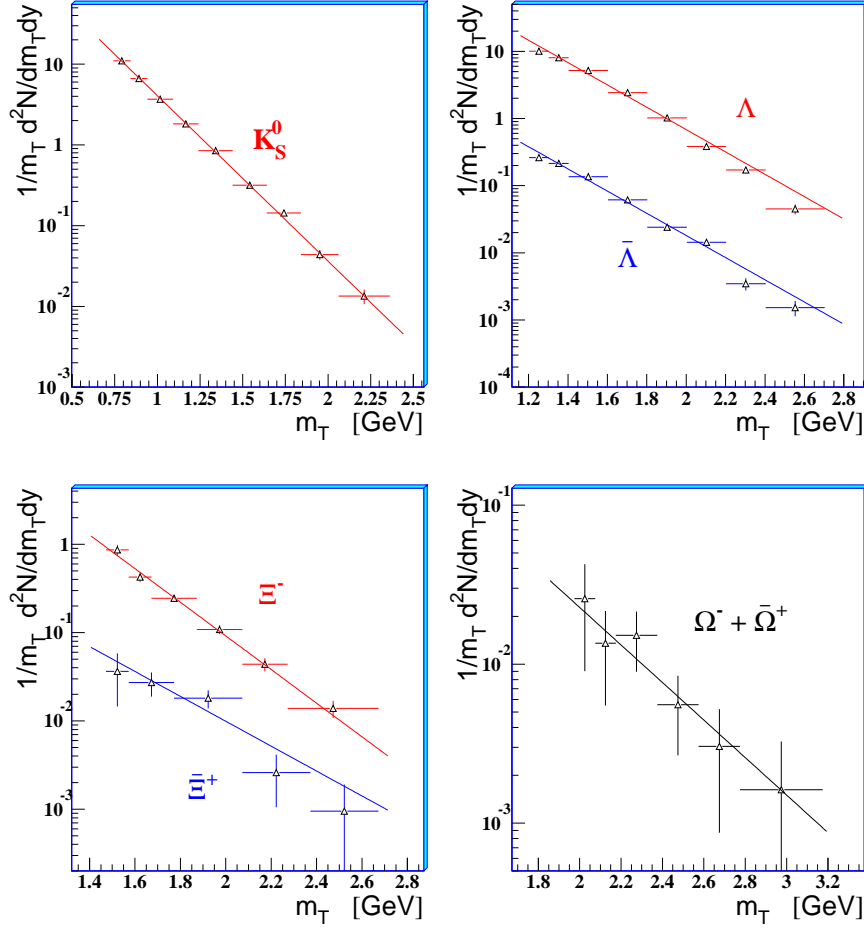


**Figure 5.** Transverse mass spectra of strange particles for the most central 53% of the Pb–Pb inelastic cross-section. The superimposed exponential functions have inverse slopes equal to the  $T_{\text{app}}$  values obtained from the maximum likelihood fits.

**Table 3.** Inverse slope parameter  $T_{\text{app}}$  (MeV) of the strange particles in the full centrality range (0–53%). The first error is statistical, the second one systematic.

$K_S^0$	$\Lambda$	$\bar{\Lambda}$
$212 \pm 3 \pm 21$	$261 \pm 4 \pm 26$	$263 \pm 6 \pm 26$
$\Xi^-$	$\bar{\Xi}^+$	$\Omega^- + \bar{\Omega}^+$
$228 \pm 12 \pm 23$	$308 \pm 63 \pm 31$	$368 \pm 120 \pm 40$

The  $\Lambda$  and  $\bar{\Lambda}$  distributions have very similar inverse slopes, agreeing within 2%§. A similar baryon–anti-baryon symmetry was reported at top SPS energy for central and

§ The systematic errors do not play a role in such a comparison since they essentially cancel out in the ratio of the spectra. The only different contribution which can be envisaged arises from the different residual background. This has been estimated to affect by less than 1.5% the inverse slope of the  $\bar{\Lambda}$ , as mentioned before.

semi-central Pb–Pb collisions for  $\Lambda$  and  $\Xi$  [14]. The similarity of baryon and anti-baryon  $m_T$  slopes is interpreted as suggestive that strange baryons and anti-baryons would be produced and evolve in the collision dynamics by similar mechanisms. Based on the  $\Lambda$  and  $\bar{\Lambda}$  results presented above, a similar conclusion can be extended to the 40 A GeV/c collisions. The large statistical errors associated to the  $\bar{\Xi}^+$   $m_T$  distribution prevent any such conclusion for this multi-strange baryon.

In the hydro-dynamical view, the apparent temperature depends on  $m_T$ ||. At a given  $m_{T0}$  value, it can be calculated according to the formula [13]:

$$T_{\text{app}}(m_{T0}) = \left[ \lim_{m_T \rightarrow m_{T0}} \frac{d}{dm_T} \left( \ln \frac{dN}{dm_T^2} \right) \right]^{-1} \quad (4)$$

With some approximations, this expression simplifies for two asymptotic cases: at low  $p_T$ , i.e.  $m_T \rightarrow m_0$ , it provides  $T_{\text{app}} = T + \frac{1}{2}m_0\langle\beta_\perp\rangle^2$  [13, 20], where  $T$  is the freeze-out temperature and  $\langle\beta_\perp\rangle$  is the average transverse flow velocity; at high  $p_t$ , i.e.  $m_T \rightarrow \infty$ , the apparent temperature is simply blue-shifted by the collective dynamics, independently of the particle mass [13]:

$$T_{\text{app}} = T \sqrt{\frac{1 + \langle\beta_\perp\rangle}{1 - \langle\beta_\perp\rangle}}. \quad (5)$$

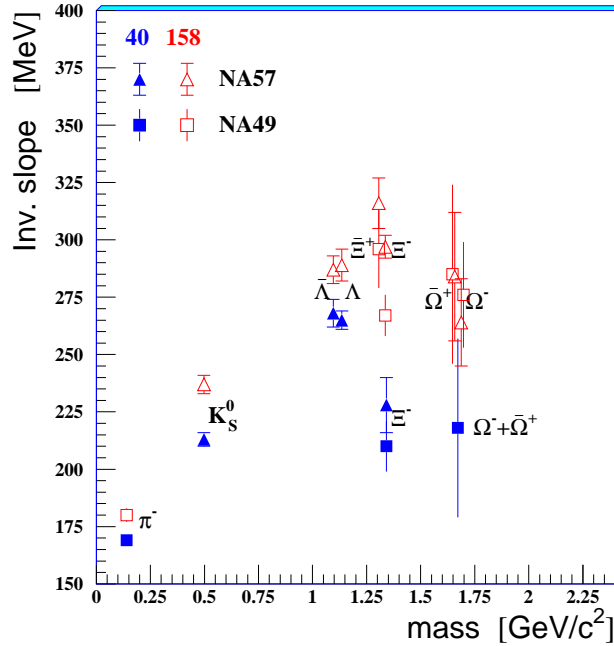
Therefore, the apparent temperature actually depends on the  $m_T$  range where the  $1/m_T dN/dm_T$  distribution has been fitted to an exponential function. Nevertheless, provided that the spectra are measured at intermediate  $p_T$  over similar  $m_T - m_0$  ranges, the inverse slopes should follow a hierarchy with the rest mass of the particles. The apparent temperature of the  $\Xi^-$  hyperon is found to be smaller than those of the  $\Lambda$  and  $\bar{\Lambda}$  particles, and of the same order as that of the  $K_S^0$  meson. A similar ‘‘violation’’ of the mass hierarchy was reported for the triply-strange  $\Omega$  particle by the WA97 [21], NA57 [14] and NA49 [22] experiments at 158 A GeV/c, and was interpreted [23] as an indication of an earlier decoupling of that particle from the expanding fireball. In the next section we shall discuss in more details the possibility of a similar effect for the  $\Xi^-$  at 40 A GeV/c.

Figure 6 shows a comparison of the inverse slopes measured at the two energies plotted as a function of the particle rest mass. The inverse slopes are lower at lower energy by about 7% for non-strange and singly-strange particles and about 20% for the multi-strange ones.

#### 4.1. Centrality dependence

The transverse mass spectra measured in the individual centrality classes of table 1 are shown in figure 7 for  $K_S^0$ ,  $\Lambda$ ,  $\bar{\Lambda}$  and  $\Xi^-$ . For the rarer  $\bar{\Xi}^+$  and  $\Omega$  hyperons, the collected statistics do not allow to study the centrality dependence. Maximum likelihood exponential fits are superimposed to the spectra, as in figure 5. The inverse slope parameters  $T_{\text{app}}$  are given in table 4 as a function of centrality.

|| In this view, the graphical interpretation of  $T_{\text{app}}$  would be the inverse of the tangent to the invariant  $1/m_T dN/dm_T$  distribution. See reference [14] for a detailed discussion.



**Figure 6.** Apparent temperature as a function of the particle rest mass in Pb–Pb at 40 A GeV/c (closed symbols, in blue on-line) as compared to 158 A GeV/c (open symbols, in red). NA49 results for negative pions [8] and multi-strange hyperons [24, 22, 25] are also shown (squares). For display purpose the ordinate scale has been zero-suppressed.

**Table 4.** Inverse slopes (MeV) of the  $m_T$  distributions of  $K_S^0$ ,  $\Lambda$ ,  $\bar{\Lambda}$  and  $\Xi^-$  as a function of centrality at 40 A GeV/c. Only statistical errors are shown. Systematic errors are estimated to be 10% for all centralities.

	0	1	2	3	4
$K_S^0$	$194 \pm 12$	$216 \pm 7$	$209 \pm 5$	$219 \pm 6$	$209 \pm 7$
$\Lambda$	$208 \pm 12$	$255 \pm 9$	$264 \pm 7$	$260 \pm 7$	$279 \pm 9$
$\bar{\Lambda}$	$186 \pm 17$	$248 \pm 12$	$257 \pm 11$	$303 \pm 15$	$276 \pm 16$
$\Xi^-$	$235 \pm 67$	$230 \pm 30$	$255 \pm 26$	$222 \pm 20$	$206 \pm 22$

An increase of the apparent temperature when going from class 0 to class 1 is observed for the singly-strange particles. Then, from class 1 to 4, the inverse slopes of these particles remain approximately constant. The baryon–anti-baryon symmetry in the shape of the spectra discussed above for the  $\Lambda$  hyperon is preserved also as a function of centrality.

No centrality dependence is observed within the errors for the  $\Xi^-$  hyperon. Remarkably, the apparent temperature of the  $\Xi^-$  hyperon is below those of  $\Lambda$  and  $\bar{\Lambda}$  and compatible with that of the light  $K_S^0$  meson for all centrality classes apart for class 0 where the mass hierarchy appears to be reestablished.

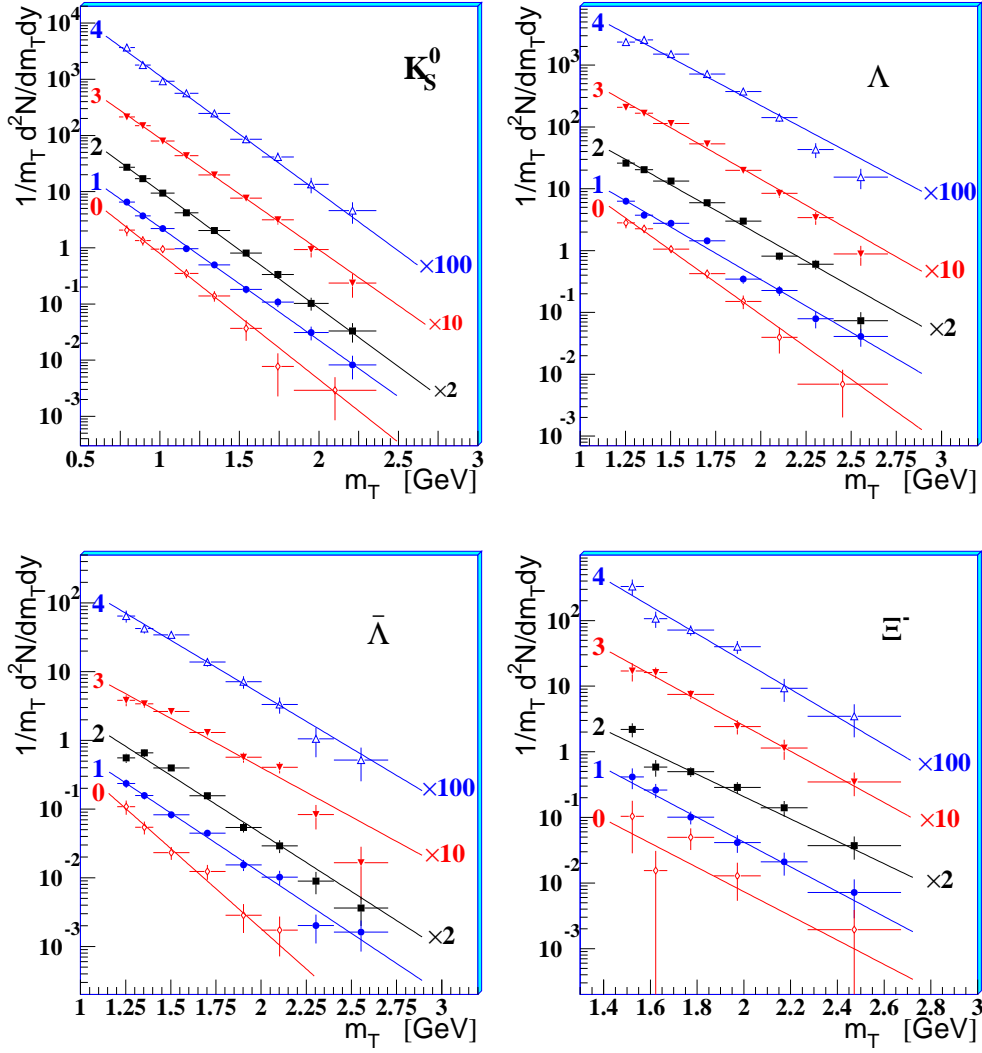


**Figure 7.** Transverse mass spectra of  $K_S^0$ ,  $\Lambda$ ,  $\bar{\Lambda}$  and  $\Xi^-$  in Pb–Pb collisions at 40 A GeV/c for the five centrality classes of table 1. For each species, class 4 is displayed uppermost and class 0 lowermost. The spectra of class 2, 3 and 4 have been scaled by factor 2, 10 and 100, respectively, for display purposes.

## 5. Blast-wave description of the spectra

In this section we employ the statistical hadronization model of reference [13], which has provided a good description of the 158 A GeV/c results [14, 19], to study the strange particle  $m_T$  spectra discussed above. The model assumes that particles decouple from a system in local thermal equilibrium with a temperature  $T$ , and which expands both longitudinally and in the transverse direction; the longitudinal expansion is taken to be boost-invariant and the transverse expansion is defined in terms of a transverse velocity profile. In this model the differential cross-section for particle  $j$  has the form:

$$\frac{1}{m_T} \frac{d^2 N_j}{dm_T dy} = \mathcal{A}_j \int_0^{R_G} m_T K_1 \left( \frac{m_T \cosh \rho}{T} \right) I_0 \left( \frac{p_T \sinh \rho}{T} \right) r dr \quad (6)$$

where  $\rho(r) = \tanh^{-1} \beta_\perp(r)$  is a transverse boost,  $K_1$  and  $I_0$  are modified Bessel functions,  $R_G$  is the transverse geometric radius of the source at freeze-out and  $\mathcal{A}_j$  is a normalization constant. The transverse velocity profile  $\beta_\perp(r)$  has been parameterized as

$$\beta_\perp(r) = \beta_S \left[ \frac{r}{R_G} \right]^n \quad r \leq R_G \quad (7)$$

The numerical value of  $R_G$  does not influence the shape of the spectra but just the absolute normalization (i.e. the constant  $\mathcal{A}_j$ ). The parameters which can be extracted from the fit of equation 6 to the experimental spectra are thus the thermal freeze-out temperature  $T$  and the surface transverse flow velocity  $\beta_S$ . Assuming a uniform particle density, the latter can be related to the *average* transverse flow velocity using the expression  $\langle \beta_\perp \rangle = \frac{2}{2+n} \beta_S$ .

Equation 6, which is obtained by integrating the Cooper–Frye invariant distribution function [26] over the rapidity of fluid elements ( $\eta$ ) up to a maximum longitudinal flow  $\eta_{\max}$  [13], is a good approximation of a full hydro-dynamical calculation for small rapidity windows about mid-rapidity. When such a hypothesis is not fulfilled, a numerical integration should be performed which, however, requires *a priori* knowledge of the maximum longitudinal flow¶. The smaller the values of the longitudinal flow, the larger the deviations from equation 6. In order to estimate the maximum bias introduced by this approximation, we have performed the integration by assuming that the longitudinal flow has the same strength as the transverse one, whereas the collective expansion is expected to be stronger in the longitudinal direction due to the incomplete stopping of the incoming nucleons. Both freeze-out parameters  $T$  and  $\langle \beta_\perp \rangle$  are found to be smaller by 2% when the full integration is performed.

### 5.1. Global fit with different profiles

The result of the global fit of equation 6 with a linear profile hypothesis (i.e. with the exponent  $n = 1$  in equation 7) to the data points of all measured strange particle spectra is shown in figure 8 (left panel) for the event sample corresponding to the most central 53% of the inelastic Pb–Pb cross-section; the fit yields the following values for the two parameters  $T$  and  $\langle \beta_\perp \rangle$ :

$$T = 118 \pm 5(\text{stat})_{-10}^{+11}(\text{syst})\text{MeV}, \quad \langle \beta_\perp \rangle = 0.392 \pm 0.010(\text{stat})_{-0.015}^{+0.013}(\text{syst})$$

with  $\chi^2/\text{ndf} = 77/40$ . A large contribution to the  $\chi^2$  comes from the  $\Xi$  spectra: the possibility of an early freeze-out of multi-strange particles is discussed below.

The  $T$  and  $\langle \beta_\perp \rangle$  parameters are statistically anti-correlated, as can be seen from the confidence level contour shown in figure 8 (right panel). The systematic errors on  $T$  and  $\langle \beta_\perp \rangle$  are instead correlated.

The results of the fits with different profile hypotheses are given in table 5. Contrary to the 158 A GeV/c case [14], where the use of the three profiles  $n=0, 1/2$  and 1 results in

¶ The  $\eta_{\max}$  can be derived from a fit to the  $dN/dy$  distributions as shown, e.g., in reference [19].

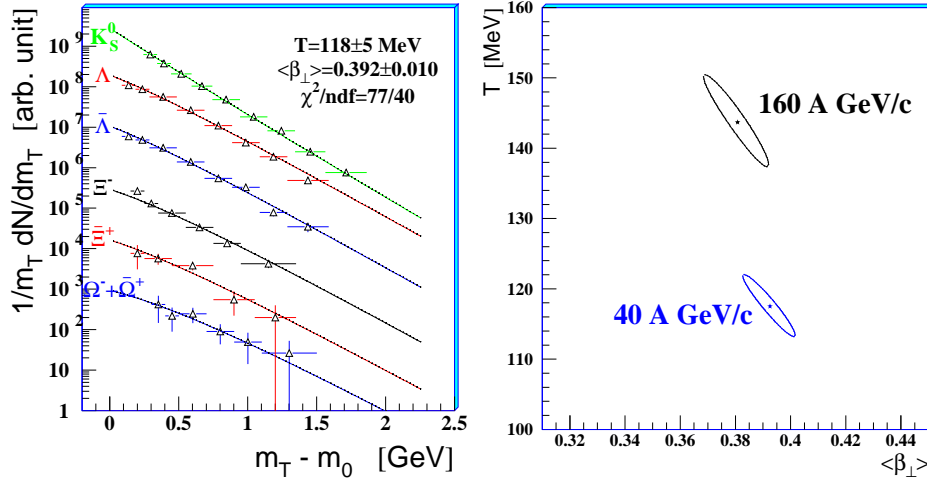


**Figure 8.** Left: blast-wave fits to the transverse mass spectra of strange particles for the most central 53% of the Pb–Pb inelastic cross-section at 40 A GeV/c. Right: contour plots in the  $T$ – $\langle\beta_{\perp}\rangle$  plane at the  $1\sigma$  confidence level as compared to the result at 158 A GeV/c [14] in the same centrality range.

**Table 5.** Results of the blast-wave model fit using different transverse velocity profiles. The quoted errors are statistical. The systematic errors on the temperature and on the velocity are estimated to be about 11% and 4%, respectively, for all four profiles.

	$n = 0$	$n = 1/2$	$n = 1$	$n = 2$
$T$ (MeV)	$125 \pm 4$	$121 \pm 4$	$118 \pm 5$	$135 \pm 10$
$\langle\beta_{\perp}\rangle$	$0.434 \pm 0.011$	$0.422 \pm 0.011$	$0.392 \pm 0.010$	$0.302 \pm 0.016$
$\chi^2/\text{ndf}$	41/40	51/40	77/40	167/40

equally well described spectra<sup>+</sup> with similar values of the freeze-out temperature and of the average transverse flow velocity, at this energy the quality of the fit is best with  $n = 0$  and gradually worsens as the exponent  $n$  is increased. Since the case  $n = 0$  is unphysical, the choice  $n = 1/2$ , which has also been suggested to be a good approximation of the full hydro-dynamical calculation [27], appears to be favoured. However, for the sake of comparison with the higher energy results, in the following a linear ( $n = 1$ ) radial dependence of the transverse flow velocity is used.

The  $1\sigma$  contour plot in the freeze-out parameter space is compared to the 158 A GeV/c result [14] in the right-hand panel of figure 8. A lower thermal freeze-out temperature is measured at the lower beam energy, while the transverse flow velocities are found to be compatible within the errors.

<sup>+</sup> The profile  $n = 2$  was instead disfavoured by data.

### 5.2. Particles with/without quarks in common with the nucleon.

Since the particles which share valence quarks with the nucleons may have a different behaviour from which do not, we have performed separate fits for the particles of the two groups. Results of separate blast-wave fits are given in table 6. The freeze-out

**Table 6.** Thermal freeze-out temperature and average transverse flow velocity in the full centrality range. The first error is statistical, the second one systematic.

particles	$T$ (MeV)	$\langle\beta_{\perp}\rangle$	$\chi^2/\text{ndf}$
$K_S^0, \Lambda, \Xi^-$	$120 \pm 7 \pm 13$	$0.39 \pm 0.02 \pm 0.02$	56.2/21
$\bar{\Lambda}, \Xi^+, \Omega^-, \bar{\Omega}^+$	$80 \pm 22 \pm 11$	$0.45 \pm 0.03 \pm 0.02$	14.8/17

conditions for the two groups of particles are compatible within  $2\sigma$ . Since the interaction cross-sections for the particles of the two groups are expected to be very different, this finding would suggest limited importance of final state interactions (i.e. a rapid thermal freeze-out) and similar production mechanisms for the two groups. A similar conclusion has also been drawn at 158 A GeV/c [14], where the freeze-out parameters for the two groups agree within  $1\sigma$ .

### 5.3. Earlier freeze-out of multi-strange particles ?

At higher energies it has been argued that multi-strange baryons may undergo an earlier freeze-out than other particles: at top SPS energy this scenario has been suggested based on the  $\Omega$  spectra measurements of the WA97 [21], NA57 [14] and NA49 [22] Collaborations. At RHIC, results from the STAR Collaboration [28] suggest that the  $\Xi$  particles freezes out earlier than  $\pi$ , K, p and  $\Lambda$ .

The  $1\sigma$  contours of the separate blast-wave fits for singly and multiply-strange particles are shown in the left-hand panel of figure 9. The plot seems to indicate that the  $\Xi^-$  hyperon, which statistically dominates the multiply-strange particle fit, may have a different thermal freeze-out behaviour from  $K_S^0$ ,  $\Lambda$  and  $\bar{\Lambda}$ . However, due to the low statistics, it is not possible to extract significant values for both freeze-out parameters from the  $\Xi^-$  spectrum alone. The possibility of a deviation for the  $\Xi^-$  hyperon from the freeze-out systematics extracted from the combined fit to the  $K_S^0$ ,  $\Lambda$  and  $\bar{\Lambda}$  spectra can be better inferred from the integrated information of the  $\Xi^-$  spectrum, i.e. from its inverse slope. In figure 9 (right panel) we plot a compilation of data\* on the  $m_T$  inverse slopes measured in Pb–Pb collisions at 40 A GeV/c, superimposed to the blast-wave model results. The full lines represent the inverse slope one would obtain by fitting an exponential to a “blast-like”  $1/m_T dN/dm_T$  distribution (i.e. to equation 6) for a generic particle of mass  $m_0$ , in the common range  $0.05 < m_T - m_0 < 1.50$  GeV/c<sup>2</sup>, for

\* The NA49 results are taken from the following references:  $\pi^-$ ,  $K^+$  and  $K^-$  from [8]; p and deuteron from [29];  $\Lambda$  and  $\bar{\Lambda}$  from [9];  $\phi$  from [30];  $\Xi^-$  from [24] and  $\Omega$  from [22]. The CERES inverse slopes, which are taken from reference [31], are shown for negative hadrons, net proton and  $\Lambda$ .

two different freeze-out conditions. The first corresponds to the parameters of the best fit to the singly-strange particles ( $T = 115$  MeV,  $\langle\beta_\perp\rangle = 0.40$ ), the second to those of the multiply-strange ones ( $T = 170$  MeV,  $\langle\beta_\perp\rangle = 0.24$ ). Since the inverse slope is a function of the  $m_T - m_0$  range where the fit is performed, we have also computed the blast-wave inverse slopes of  $K_S^0$ ,  $\Lambda$  and  $\Xi$  spectra in the  $m_T - m_0$  ranges of NA57 (closed circles). The measured values of the inverse slope of the multi-strange baryons appear to deviate significantly from the trend of the other strange particles.

#### 5.4. Centrality dependence

The hydro-dynamical description of observables related to collective dynamics, e.g. the elliptic flow, is strongly influenced by the freeze-out temperature. It is therefore important to determine how the thermal freeze-out conditions may change with respect to the initial collision geometry.

The centrality dependence of the freeze-out parameters at 158 A GeV/c beam momentum can be summarized as follows: the more central the collisions the larger the transverse collective flow and the lower the final thermal freeze-out temperature [14], the dependence being more pronounced for the flow. A similar behaviour was reported at RHIC by the PHENIX [32], STAR [28] and BRAHMS [33] Collaborations. Higher freeze-out temperatures for more peripheral collisions may be interpreted as the result of earlier decoupling of the expanding system.

In figure 10 we show the  $1\sigma$  confidence level contours for each of the five centrality classes defined in table 1. With decreasing collision centrality the transverse flow velocity

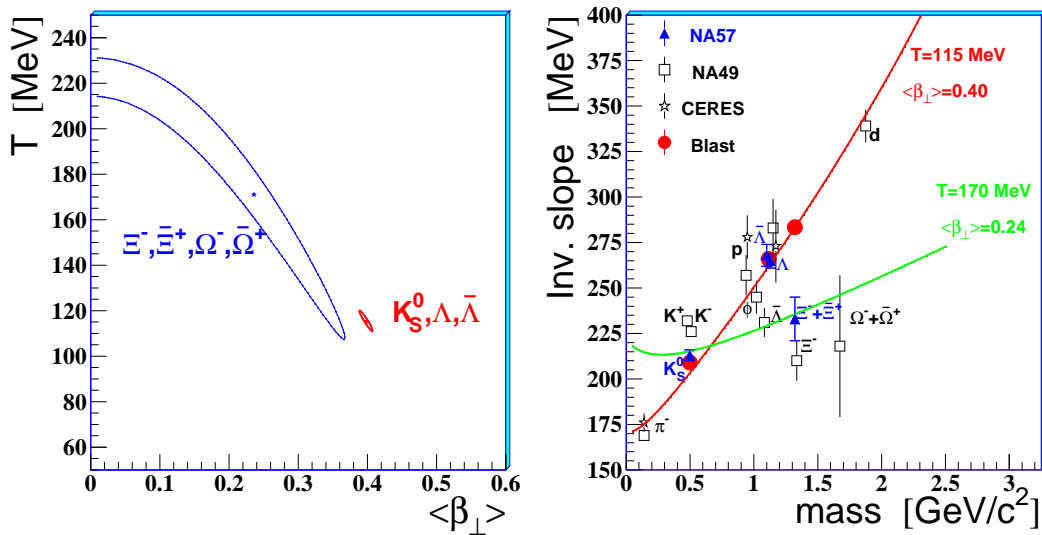


**Figure 9.** Left: the thermal freeze-out temperature versus the average transverse flow velocity for blast-wave fits using a linear ( $n = 1$ ) velocity profile. The  $1\sigma$  contours are shown, with the markers indicating the optimal fit locations. Right: prediction of the blast-wave model for inverse slopes (see text for details).



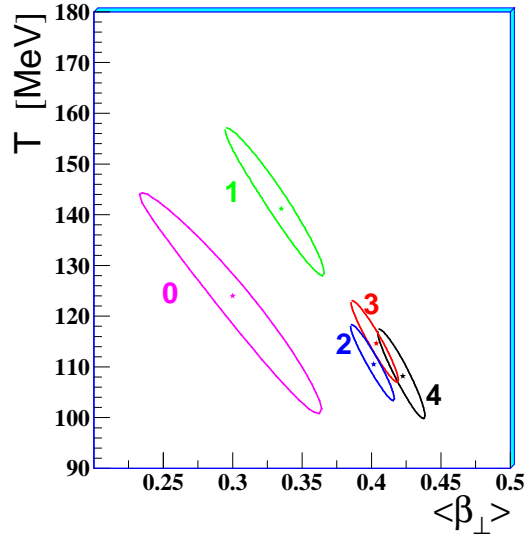


**Figure 10.** The  $1\sigma$  confidence level contours from fits in each centrality class.

decreases steadily, as also observed at higher energies. The freeze-out temperature is roughly constant within the errors at the value  $T \approx 110 \pm 10$  MeV for the three most central classes (i.e. for the most central 23% of the inelastic Pb–Pb cross-section).

## 6. Conclusions

We have analyzed the transverse mass spectra of  $\Lambda$ ,  $\Xi^-$ ,  $\Omega^-$  hyperons, their anti-particles and  $K_S^0$  mesons in Pb–Pb collisions at 40 A GeV/c beam momentum over a centrality range corresponding to the most central 53% of the Pb–Pb inelastic cross-section.

The inverse slopes of these particles are found to be lower than those measured at 158 A GeV/c beam momentum. As a function of centrality, the inverse slopes of the singly-strange particles increase significantly when going from the most peripheral class to the next one; for the more central classes, a weak increase with centrality cannot be excluded for  $\Lambda$  and  $\bar{\Lambda}$ . The inverse slope of the  $\Xi^-$  is compatible with being constant over the whole centrality range.  $\bar{\Xi}^+$  and  $\Omega$  hyperons have not been studied as a function of the centrality due to the limited statistics.

Particle and anti-particle inverse slopes are compatible within the errors; in particular, the inverse slopes of  $\Lambda$  and  $\bar{\Lambda}$  hyperons are the same within 5% over the covered centrality range, thus suggesting that strange baryons and anti-baryons may be produced and evolve in the collision dynamics by similar mechanisms.

The inverse slope of the  $\Xi^-$  hyperons significantly deviates from the general trend of values increasing with the particle rest mass, as observed for non-strange and singly-strange particles.

The analysis of the transverse mass spectra in the framework of the blast-wave model suggests that after a central collision the system expands with an average

transverse flow velocity of about 40% of the speed of light and then it freezes out when the temperature is of the order of 110 MeV. The measured transverse flow velocity is compatible with that measured at 158 A GeV/c but the freeze-out temperature is lower at low energy. The inverse slope of the  $\Xi^-$  hyperon deviates from the value predicted by the blast-wave model tuned on singly-strange particles ( $K_S^0$ ,  $\Lambda$  and  $\bar{\Lambda}$ ). Finally, the results on the centrality dependence of the expansion dynamics indicate that with increasing centrality the transverse flow velocity increases steadily and the freeze-out temperature decreases when going from class 1 (23–40%) to the more central classes.

## References

- [1] Karsch F 2002 *Lect. Notes Phys.* **583** 209
- [2] Ritter H G and Wang X-N (ed) 2004 *J. Phys. G: Nucl. Phys.* **30** S633-S1430 (*Proc. Quark Matter 2004*)  
Lévai P and Csörgo T (ed) 2006 *Nucl. Phys. A* in press (*Proc. Quark Matter 2005*)
- [3] Rafelski 2004 *J. Phys. G: Nucl. Phys.* **30** S1-S28
- [4] Rafelski J and Müller B 1982 *Phys. Rev. Lett.* **48** 1066  
Rafelski J and Müller B 1986 *Phys. Rev. Lett.* **56** 2334  
Koch P, Müller B and Rafelski J 1986 *Phys. Rep.* **142** 167  
Rafelski J 1991 *Phys. Lett. B* **262** 333
- [5] Antinori F *et al.* 2006 *J. Phys. G: Nucl. Phys.* **32** 427-441
- [6] Andersen E *et al.* 1999 *Phys. Lett. B* **449** 401  
Antinori F *et al.* 1999 *Nucl. Phys. A* **661** 130c
- [7] Bruno G E *et al.* 2004 *J. Phys. G: Nucl. Phys.* **30** S717-S724
- [8] Afanasiev S V *et al.* 2002 *Phys. Rev. C* **66** 054902
- [9] Antic T *et al.* 2004 *Phys. Rev. Lett.* **93** 022302
- [10] Alt C *et al.* 2005 *Phys. Rev. Lett.* **94** 052301
- [11] Andronic A, Braun-Munzinger P and Stachel J 2006 *Nucl. Phys. A* **772** in press, nucl-th/0511071  
Becattini F, M. Gaździcki M, Keranen A, Manninen J and Stock R 2004 *Phys. Rev. C* **69** 024905  
Becattini F, Manninen J and Gaździcki 2006 *Phys. Rev. C* **73** 044905  
Letessier J and Rafelski J 2005 submitted to *Phys. Rev. C*, nucl-th/0504028  
Broniowski W, Florkowski W and Michalec M 2002 *Acta Phys. Pol. B* **33** 761, nucl-th/0106009  
Broniowski W and Florkowski W 2002 *Phys. Rev. C* **65** 064905, nucl-th/0112043
- [12] Hirano T 2004 *J. Phys. G: Nucl. Phys.* **30** S845-S851  
Torrieri G and Rafelski J *J. Phys. G: Nucl. Phys.* **30** S557-S564  
Heinz U W 2005 *J. Phys. G: Nucl. Phys.* **31** S717-S724  
Csernai L P, Molnár E, Nyíri Á and Tamosiunas K 2005 *J. Phys. G: Nucl. Phys.* **31** S951-S957  
Steinberg P A 2005 *Nucl. Phys. A* **752** 423c-432c
- [13] Schnedermann E, Sollfrank J and Heinz U 1993 *Phys. Rev. C* **48** 2462  
Schnedermann E, Sollfrank J and Heinz U 1994 *Phys. Rev. C* **50** 1675
- [14] Antinori F *et al.* 2004 *J. Phys. G: Nucl. Phys.* **30** 823-840
- [15] Manzari V *et al.* 1999 *J. Phys. G: Nucl. Phys.* **25** 473  
Manzari V *et al.* 1999 *Nucl. Phys. A* **661** 761c
- [16] Antinori F *et al.* 2005 *J. Phys. G: Nucl. Phys.* **31** 321-335
- [17] Eidelman S *et al.* 2004 *Review of Particle Properties Phys. Lett. B* **592** 1
- [18] Bruno G E *et al.* 2002 in *QCD and High Energy Hadronic Interactions* edited by Trần Thanh Vân 405-410 (*Proc. 37<sup>th</sup> Rencontres de Moriond*); Preprint hep-ex/0207047
- [19] Antinori F *et al.* 2005 *J. Phys. G: Nucl. Phys.* **31** 1345-1357
- [20] Lee K S, Heinz U and Schnedermann E 1990 *Z. Phys. C* **48** 525

- Csörge T and Lorstad B 1996 *Phys. Rev. C* **54** 1390
- [21] Antinori F *et al.* 2000 *Eur. Phys. J. C* **14** 633
  - [22] Alt C *et al.* 2005 *Phys. Rev. Lett.* **94** 192301
  - [23] van Hecke H, Sorge H and Xu N 1998 *Phys. Rev. Lett.* **81** 5764
  - [24] Afanasiev S V *et al.* 2002 *Phys. Lett. B* **538** 275-281
  - [25] Meurer C *et al.* 2004 *J. Phys. G: Nucl. Phys.* **30** S1325-S1328
  - [26] Cooper F and Frye G 1974 *Phys. Rev. D* **10** 186
  - [27] Wiedemann U A 2003 *Private communication*
  - [28] Adams J. *et al.* 2004 *Phys. Rev. Lett.* **92** 182301
  - [29] Anticic T *et al.* 2004 *Phys. Rev. C* **69** 024902
  - [30] Friese V *et al.* 2005 *J. Phys. G: Nucl. Phys.* **31** S911-S918 and *private communication*
  - [31] Schmitz W *et al.* 2002 *J. Phys. G: Nucl. Phys.* **28** 1861-1868
  - [32] Adcox K *et al.* 2004 *Phys. Rev. C* **69** 024904
  - [33] Arsene I *et al.* 2005 *Phys. Rev. C* **72** 014908